THE SEISMOLOGICAL SOCIETY OF AMERICA
400 Evelyn Ave., Suite 201
Albany, CA 94706-1375
(510) 525-5474; FAX (510) 525-7204
www.seismosoc.org

Bulletin of the Seismological Society of America, Vol. 107, No. 2, pp. 624–638, April 2017, doi: 10.1785/0120160142

Improving Global Radial Anisotropy Tomography: The Importance of Simultaneously Inverting for Crustal and Mantle Structure

by Sung-Joon Chang and Ana M. G. Ferreira

Abstract Observed seismic anisotropy gives the most direct information on mantle flow, but it is challenging to image it robustly at global scales. Difficulties in separating crustal from mantle structures in particular can have a strong influence on the imaging. Here we carry out several resolution tests using both real and synthetic data, which show that unconstrained crustal structure can strongly contaminate retrieved radial anisotropy at 100–150 km depth. To efficiently reduce crustal effects, we perform whole-mantle radially anisotropic tomographic inversions including crustal thickness perturbations as model parameters. Our data set includes short-period group velocity data, which are sensitive to shallow structure. We perform a series of tests that highlight the advantages of our approach and show that to properly constrain thin oceanic crust in global radially anisotropic inversions, group velocity data with wave periods of at least $T \sim 20$ s or shorter are required. Our Moho perturbation model shows thicker crust along subduction zones and beneath the Ontong Java plateau in the southwestern Pacific than in the global crustal model CRUST2.0. These features agree well with other crustal models as well as with refraction survey data and tectonic features in these regions.

Introduction

Seismic tomography has unveiled 3D velocity structure in the Earth's interior, thereby enhancing our understanding of plate tectonics and linking surface tectonics to deeper mantle dynamics. It has been utilized to reveal not only velocity information but also seismic anisotropy, which may be used to constrain the patterns of mantle convection. Indeed, when combined with information from mineral physics on the slip systems of anisotropic mantle minerals, observed seismic anisotropy provides key information on the large-scale deformation caused by mantle dynamics (e.g., Karato *et al.*, 2008). Radial anisotropy is the simplest type of anisotropy, which can potentially help discriminate between vertical and horizontal directions of mantle flow (e.g., Ekström and Dziewoński, 1998; Gu *et al.*, 2005).

When imaging mantle structure, it is important to separate the effects of the crust on seismic data from those of the mantle, because even long-period surface waves ($T > 100$ s) are significantly affected by crustal structure (e.g., Montagner and Jobert, 1988; Bozdağ and Trampert, 2008). The so-called crustal corrections have been widely used in global tomography since the first global tomography studies (e.g., Woodhouse and Dziewonski, 1984), whereby the theoretical crustal effects are subtracted from the seismic measurements before inverting for mantle structure. This approach has been a popular alternative to difficult simultaneous inversions for global crustal and mantle structure due to their substantial scale differences. However, crustal effects can be highly nonlinear (e.g., Kustowski *et al.*, 2007; Marone and Romanowicz, 2007), and it is well known that existing global crustal models typically used for such crustal corrections (e.g., CRUST2.0; Bassin *et al.*, 2000) can contain imperfections. For example, crustal structure of data-poor regions is obtained by extrapolating information from similar tectonic provinces with lots of data, potentially leading to errors.

The imaging of radial anisotropy in the mantle is particularly sensitive to crustal effects. For example, simply changing the model used for crustal corrections in inversions for radial anisotropy can impact the data fit as much as allowing for lateral variations in radial anisotropy (Ferreira *et al.*, 2010). Because of this difficulty, some researchers prefer to build smooth, long-wavelength equivalent crustal models that fit the data (Fichtner *et al.*, 2009; Lekić and Romanowicz, 2011; French and Romanowicz, 2014), whereas others invert for mantle and crustal structure globally with Monte Carlo techniques (Shapiro and Ritzwoller, 2002) or use full-wavefield numerical methods at regional scales (Chen *et al.*, 2015; Zhu *et al.*, 2015). Moreover, Lebedev *et al.* (2013) highlight the strong trade-off between crustal thickness and velocity in surface-wave data inversions. They suggest a Moho depth inversion strategy whereby the use of *a priori* information on crustal and mantle structure enables enhanced Moho mapping.

Recently, a new global radially anisotropic whole-mantle model SGLOBE-rani has been built using a massive seismic

data set (Chang *et al.*, 2015), which revealed new features about the Earth's deep interior (Chang *et al.*, 2016). To better constrain radial anisotropy, notably by addressing the crustal correction problem in global tomography, Chang *et al.* (2014, 2015) included crustal thickness perturbations from CRUST2.0 (Bassin *et al.*, 2000) as model parameters as well as shear-wave velocity and radial anisotropy perturbations in their tomographic linearized inversions. For this purpose, they used short-period group velocity data (Ritzwoller and Levshin, 1998) with a period range down to $T \sim 16$ s along with a large set of longer period surface-wave phase velocity measurements as well as body-wave travel-time data. Thus, the ultimate goal of SGLOBE-rani was to improve global anisotropic tomography through simultaneous inversions for Moho depth as well as for isotropic and anisotropic shear-wave velocity parameters.

In this study, we perform resolution tests with both synthetic and real data to assess the performance of joint inversions for crustal thickness, mantle isotropic and radially anisotropic structure at separating crustal and mantle effects. We quantify the influence of unconstrained crustal structure on retrieved radial anisotropy in the mantle. Moreover, to efficiently reduce crustal effects, we carry out resolution tests to determine which wave period range of group velocity data is needed to avoid crustal-mantle contamination in the inversions. Then, we compare the Moho depth perturbations obtained from SGLOBE-rani with the global crustal models CRUST1.0 (Laske *et al.*, 2013), CRUST07 (Meier *et al.*, 2007), and LITHO1.0 (Pasyanos *et al.*, 2014), and with seismic refraction survey data to investigate their consistency with other models and observations.

Data and Modeling

In this section, we briefly summarize the strategy used to build SGLOBE-rani and its associated crustal thickness perturbations (Chang *et al.*, 2015), which underlies the various synthetic and real data tests undertaken in this study. The data set used consists of ~43,000,000 surface-wave fundamental-mode and overtone dispersion measurements and ~420,000 body-wave teleseismic travel-time data, which have complementary lateral and vertical sensitivity to mantle structure (see Chang *et al.*, 2015, for a full description and references of the data used). Among this data set, fundamental-mode group velocity data (Ritzwoller and Levshin, 1998) play an essential role in constraining crustal structure, because they are more sensitive to shallow structure than phase velocity data (e.g., Lebedev *et al.*, 2013). The period range of the group velocity data is from $T \sim 16$ to 150 s for Rayleigh waves and from $T \sim 16$ to 100 s for Love waves, respectively. The shortest period of fundamental-mode phase velocity data we used is $T \sim 25$ s (Chang *et al.*, 2015).

We expanded the model horizontally with spherical harmonic basis functions up to degree 35, corresponding to a lateral grid distance of ~6°. Hence, a total of 1296 model parameters are associated with crustal thickness perturbations. Our strategy to model crustal structure comprises two main steps. We first apply crustal corrections to all data using the CRUST2.0 crustal model superimposed on preliminary reference Earth model (PREM's) mantle structure (Dziewoński and Anderson, 1981). While the body-wave travel-time corrections are obtained from cross correlations on normal-mode summation theoretical seismograms (Ritsema *et al.*, 2009), for surface waves we calculate the local predicted eigenfrequencies of the surface wave-equivalent modes in the $2° \times 2°$ grid of CRUST2.0. The path-integrated predicted crustal signals based on the great-circle approximation are then subtracted from the measured eigenfrequency for each path. We take into account nonlinear effects of crustal structure on surface-wave dispersion data by exactly calculating local eigenfrequencies using normal-mode theory (e.g., Takeuchi and Saito, 1972). Second, the corrected data are jointly inverted for isotropic and radially anisotropic shear-wave perturbations with respect to PREM and for crustal thickness perturbations from CRUST2.0 given that the data are corrected for CRUST2.0. Mid-crustal discontinuity topographies are also adjusted according to the variation of the estimated crustal thickness. Sensitivity kernels with respect to crustal thickness are calculated with the formulation of Woodhouse and Dahlen (1978) for phase velocity data and by numerical differentiation for the group velocity and body-wave travel-time data. Sensitivity kernels with respect to isotropic S velocity and radial anisotropy for group velocities are calculated using the sensitivity kernels for phase velocities (Takeuchi and Saito, 1972), following Rodi *et al.* (1975). We use the PREM model as the 1D starting model and the tomographic inversions are carried out using a damped least-squares inversion procedure (Ferreira *et al.*, 2010; Chang *et al.*, 2015). Synthetic tests showed a good retrieval of realistic crustal structures (further details are given in Chang *et al.*, 2015). In addition, the use of the great-circle approximation is justified by the fact that this study focuses on phase and travel-time data. For example, recently Parisi and Ferreira (2016) showed that the great-circle approximation accurately predicts Rayleigh-wave phase information at least down to $T \sim 45$ s for realistic 3D Earth models. Regarding shorter period data, notably the short-period group velocity data used in the construction of SGLOBE-rani, these measurements are based on very strict data selection criteria (e.g., Ritzwoller and Levshin, 1998), which avoid data strongly deviating from ray theoretical predictions. Nevertheless, one should bear in mind that potential unaccounted off-great circle and finite-frequency effects are a possible caveat of our study, notably for short-period Love-wave data.

Resolution Tests

In this section, we perform various resolution tests to quantify the crustal effects on retrieved mantle radial anisotropy $\xi = (V_{SH}/V_{SV})^2$ and to determine the adequate period range of surface-wave data necessary to robustly constrain global crustal and mantle structure. We use both real and synthetic data and follow exactly the same inversion procedure as that used to build the SGLOBE-rani model.

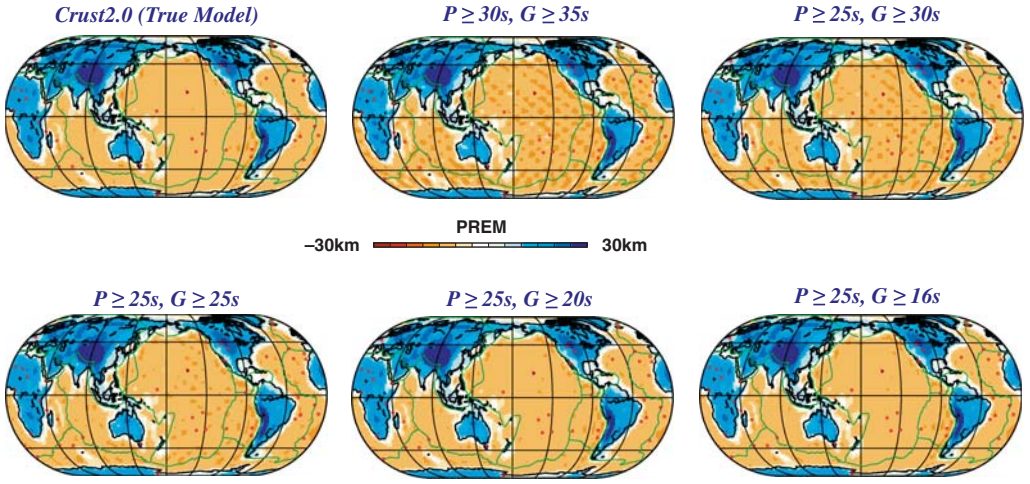

Figure 1. Resolution tests for crustal thickness variations with varying period range of the surface-wave data used in the inversions. The crustal thickness distribution from CRUST2.0 (Bassin *et al.*, 2000) is the true input model (upper-left panel), whereas the crustal thickness perturbations retrieved from the inversions are shown in the subsequent panels. Crustal thickness variations are shown with respect to preliminary reference Earth model (PREM; Dziewoński and Anderson, 1981), which has a Moho depth of 24.4 km. The titles indicate the period range used in the inversions, and P and G mean phase and group velocity data, respectively.

Testing the Effect of the Range of Wave Periods Used in the Inversions

We start by performing resolution tests whereby theoretical fundamental-mode surface-wave data with a varying period range are used in synthetic inversions (Fig. 1). The synthetic surface-wave data share the same ray paths as in our real data set. The true input model contains Moho depths as in CRUST2.0 combined with 2000 km × 2000 km checkers of 5% anomalies in the mantle. Figure 1 shows the retrieved structures. Because group velocity data are more sensitive to Moho depth than phase velocity data, and the shortest period of phase velocity data is $T \sim 25$ s in our data set (whereas the period range of group velocity data goes down to $T \sim 16$ s), group velocity data play an essential role in the resolution tests. When the shortest period of group velocity data used in the inversion is $T \geq 25$ s, checkers emerge in the retrieved crustal thickness perturbations, notably in oceanic crusts, indicating that group velocity data with $T \geq 25$ s do not resolve well thin oceanic Moho depths. This problem is alleviated when a wider period range is used in the inversions, with shorter wave periods down to $T \sim 20$ s and $T \sim 16$ s. These tests demonstrate that short-period group velocity data with wave periods down to at least $T \sim 20$ s are necessary to constrain Moho depths globally. Moreover, our tests show that the incorporation of group velocity data with an inadequate period range may lead to the contamination of retrieved crustal thickness by mantle structure.

We then performed more realistic synthetic resolution tests, also successively changing the wave period range of the surface-wave data used in the inversions, but now using the SGLOBE-rani model as input model. Figure 2 shows the retrieved results when using group velocity data with periods down to 25 s (G25 test) and 16 s (G16 test). While the model obtained using group velocity data down to 16 s shows small differences to the true model, the result using group velocity data down to 25 s depicts larger differences. As for the retrieved crustal thickness perturbations, the G25 test shows thicker oceanic crusts than the input model, whereas the G16 test recovers the anomalies almost perfectly. The same trend is observed when analyzing the retrieved radial anisotropy. The G25 test shows significant differences from the input model down to 150 km depth, whereas the G16 test performs better. Regarding results for Voigt average isotropic structure, the G25 test also performs as well as the G16 test except for 50 km depth, which means that the crust affects the recovered radially anisotropic structure more strongly than the Voigt average isotropic structure. This is probably due to the weaker sensitivity of the data to anisotropic structure than to isotropic structure, as well as to the different behaviors of sensitivity kernels of Rayleigh- and Love-wave group velocities for the depth range of crust, which will be shown later in the Discussion and Conclusions section.

Because our data and modeling uncertainties are essentially unknown, we do not add errors to the synthetic data and thus, while very instructive, our synthetic tests have some limitations. Hence, we also carried out inversions with the same real data set as used to build SGLOBE-rani, but with different wave period ranges. As explained previously, SGLOBE-rani was built by incorporating group velocity data down to $T \sim 16$ s. If we use group velocity data only down to 25 s, we obtain a different model to SGLOBE-rani (Fig. 3). While slight differences in isotropic structure are only observed at shallow depths (~50 km), differences in anisotropy persist down to ~150 km depth, showing the susceptibility of radial anisotropy to crustal effects. The differences in crustal thickness perturbations (bottom panel of Fig. 3) are similar to those obtained in the synthetic test shown in Figure 2. Beneath the eastern Pacific, the Indian Ocean, and the Atlantic Ocean, the retrieved oceanic crust gets thicker than in CRUST2.0 when using group velocity data with

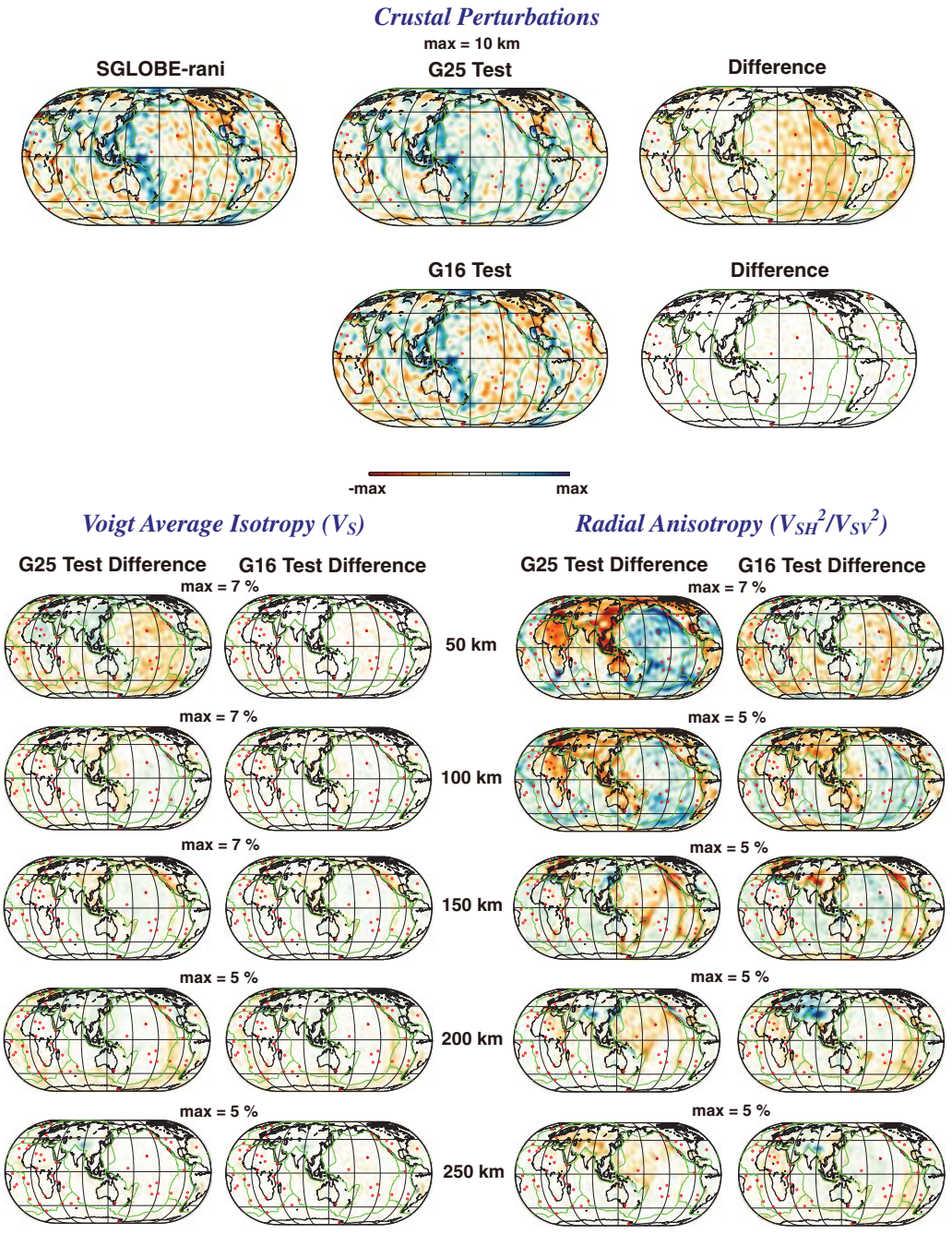

Figure 2. Two synthetic resolution tests for (top) the retrieval of crustal thickness perturbations and for (bottom) Voigt average isotropy and radial anisotropy. SGLOBE-rani is the true input model. G16 test and G25 test represent the resulting models with all group velocity data down to 16 s and 25 s, respectively. Panels named "Difference" are constructed by subtracting the output test models from SGLOBE-rani.

$T \geq 25$ s, which is not realistic. This confirms that group velocity data with $T \leq 20$ s are necessary to properly constrain oceanic crust, especially thin oceanic crusts around ridges, and to robustly image anisotropy in the mantle.

Testing the Leakage of Crustal Structure into Retrieved Mantle Structure

The previous real data resolution test showed that to both properly image crustal thickness perturbations and to reduce artificial mantle anisotropy features, it is necessary to use data with $T \leq 20$ s in our inversions. To further test whether our data set and modeling strategy can prevent the leakage of crustal structure into mantle structure, we carried out a synthetic test using the CRUST2.0 model as the true input model combined with PREM's mantle isotropic and radially anisotropic structures. Figure 4 shows that the output crustal model (left-middle side diagram) agrees well with the true model, showing little difference between them (left-bottom side diagram, with a smaller range of the scale bar).

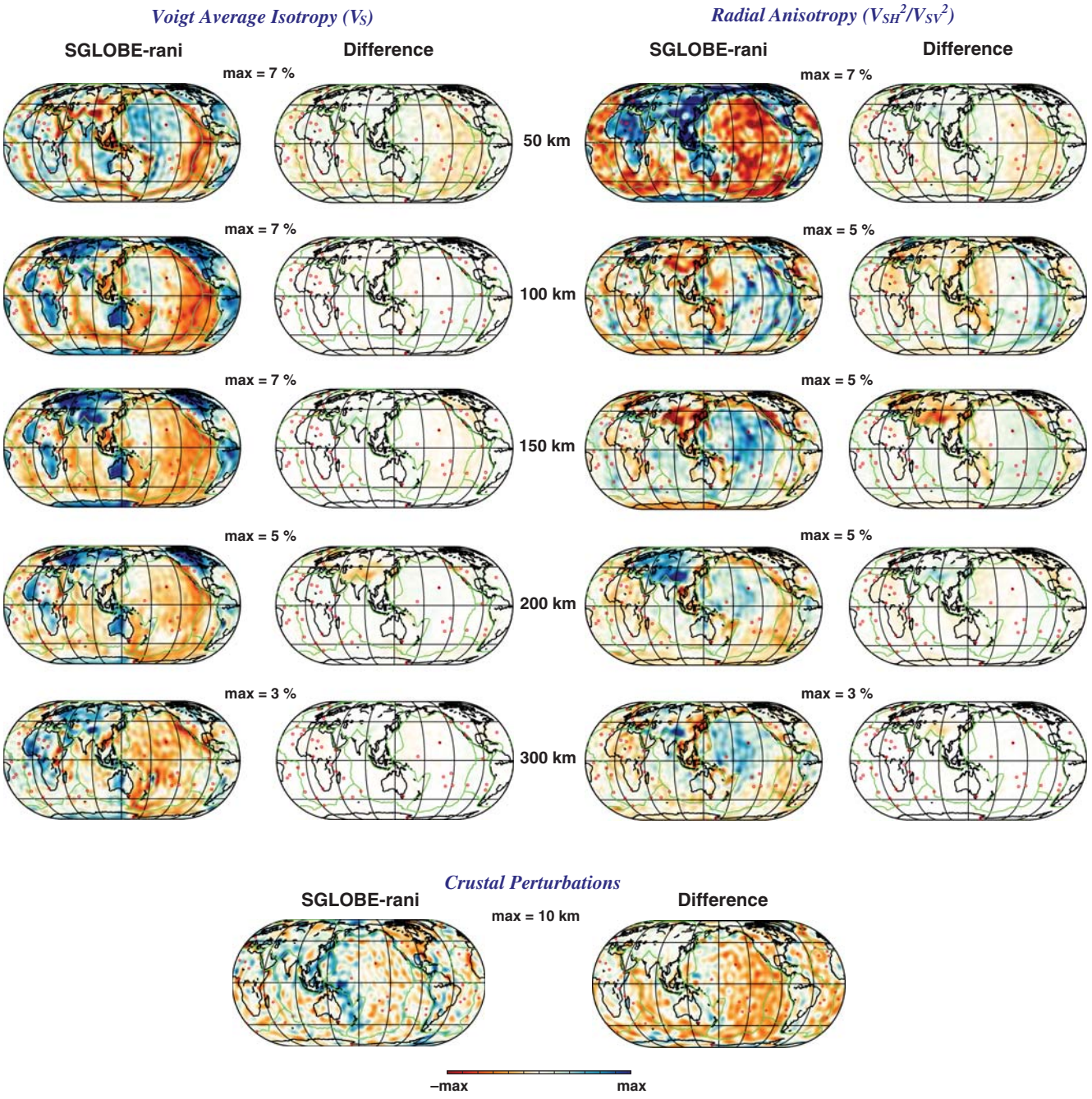

Figure 3. SGLOBE-rani and the differences between it and the output model from real data inversions excluding short-period group velocity data (less than 25 s). The first two columns correspond to the isotropic models and the next two columns are related to the anisotropic models. Crustal thickness perturbations associated with SGLOBE-rani and the differences between the two models are presented at the bottom.

Maximum crustal thickness perturbations of over 30 km are well retrieved, which is very encouraging. Indeed, such large perturbations are not expected from our real data inversions because the data are corrected for CRUST2.0. The middle and right columns of Figure 4 show depth slices of the retrieved isotropic and radially anisotropic output perturbation models, respectively, which should in principle contain no perturbations. The results show only very small mantle structure variations ($<1\%$). We observe isotropic low-velocity anomalies at ~50 km beneath Africa and the Atlantic Ocean, but the anomalies ($<1\%$) are very small compared with the actual amplitudes of the isotropic part of SGLOBE-rani at the same depth (Fig. 3; note the different ranges of the scale bars).

Finally, to investigate how unconstrained crustal structure may leak into mantle structure when using real data, we compare mantle models obtained with and without crustal thickness perturbations as model parameters in real data

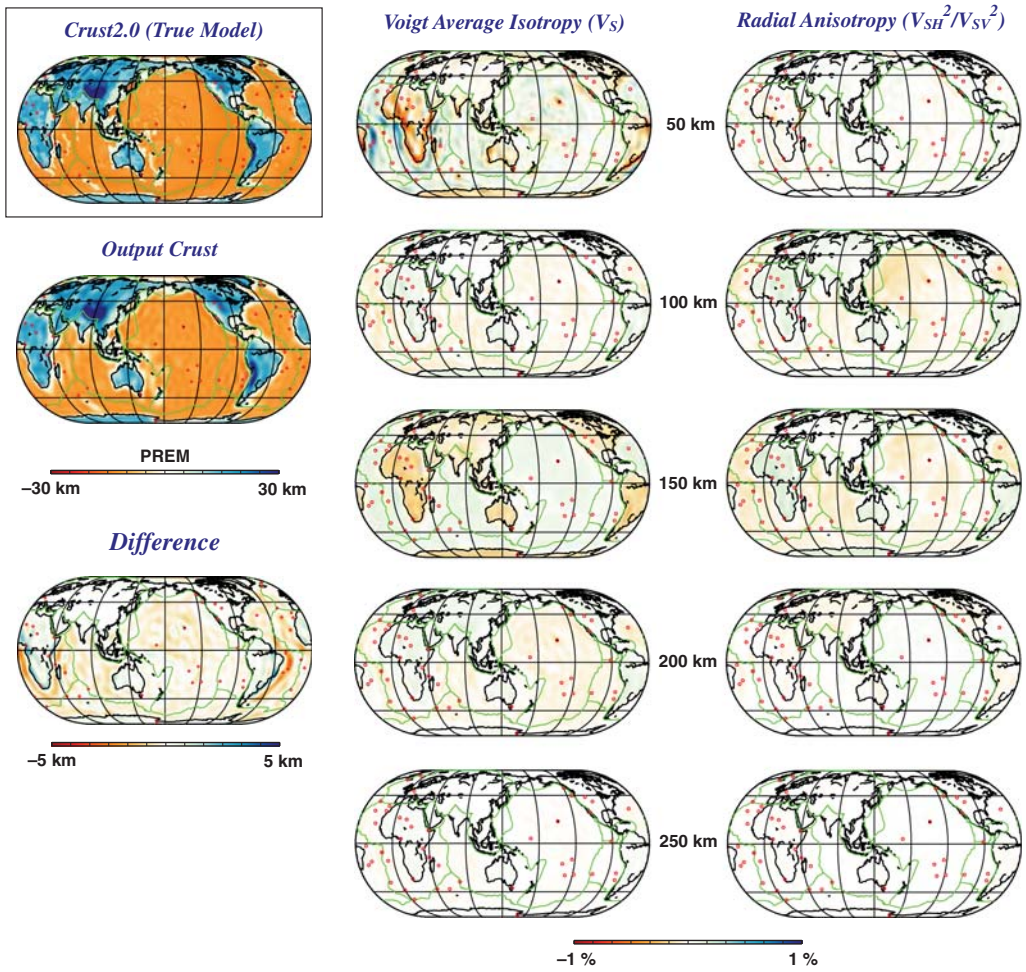

Figure 4. Synthetic resolution test investigating the leakage of crustal thickness structure into mantle velocity structure. The true input model consists of crustal thickness from CRUST2.0 and PREM's mantle velocity and radial anisotropy. The output crustal thickness model and the difference from CRUST2.0 are presented on the left-middle and left-bottom sides, respectively. In the middle and right columns, output isotropic and radial anisotropic perturbation depth slices are shown at 50, 100, and 150 km depth, respectively. The maximum and minimum of the color scale bar is ±1%.

inversions. Figure 5 shows the differences between the two models. The amplitude of the observed differences is comparable to the amplitude of anomalies in SGLOBE-rani for several regions such as Tibet, the Himalayas, Alps, subduction zones, and North America, notably at 100–150 km depth for anisotropic structure and at 150 km depth for isotropic structure. As expected, the retrieved anisotropy images are more strongly affected by unconstrained crustal structure than the isotropic images. Differences in anisotropic structure persist down to 400 km depth, with peak amplitude at 100 km depth. These strong amplitude differences highlight the importance of including crustal perturbations as model parameters in the inversions to absorb unconstrained crustal structure and to reduce spurious features in the retrieved anisotropy, notably at 100–150 km depth.

Crustal Model Comparisons

To further validate our modeling approach, in this section we compare our Moho perturbation model with previous crustal models and Moho depths from refraction surveys and receiver functions. In Figure 6, we compare our Moho depth perturbations with three previous crustal models: CRUST1.0 (Laske *et al.*, 2013), CRUST07 (Meier *et al.*, 2007), and LITHO1.0 (Pasyanos *et al.*, 2014). The four models are presented as perturbations with respect to CRUST2.0, which is also shown for reference.

CRUST1.0 is a high-resolution crustal model based on a compilation of various sources of information such as refraction survey and receiver function studies. It is an update of the CRUST2.0 (Bassin *et al.*, 2000) and CRUST5.1 (Mooney *et al.*, 1998) models, built on a $1° \times 1°$ grid by assembling observations from data-rich regions, which are extrapolated to data-poor regions with similar tectonic characteristics. CRUST07 comprises average crustal shear-wave velocity and Moho depth on a $2° \times 2°$ grid. It was built by using a neural network approach to invert $T \sim 35$–145 s fundamental-mode phase velocity data (Trampert and Woodhouse, 2003) and group velocity measurements for Rayleigh

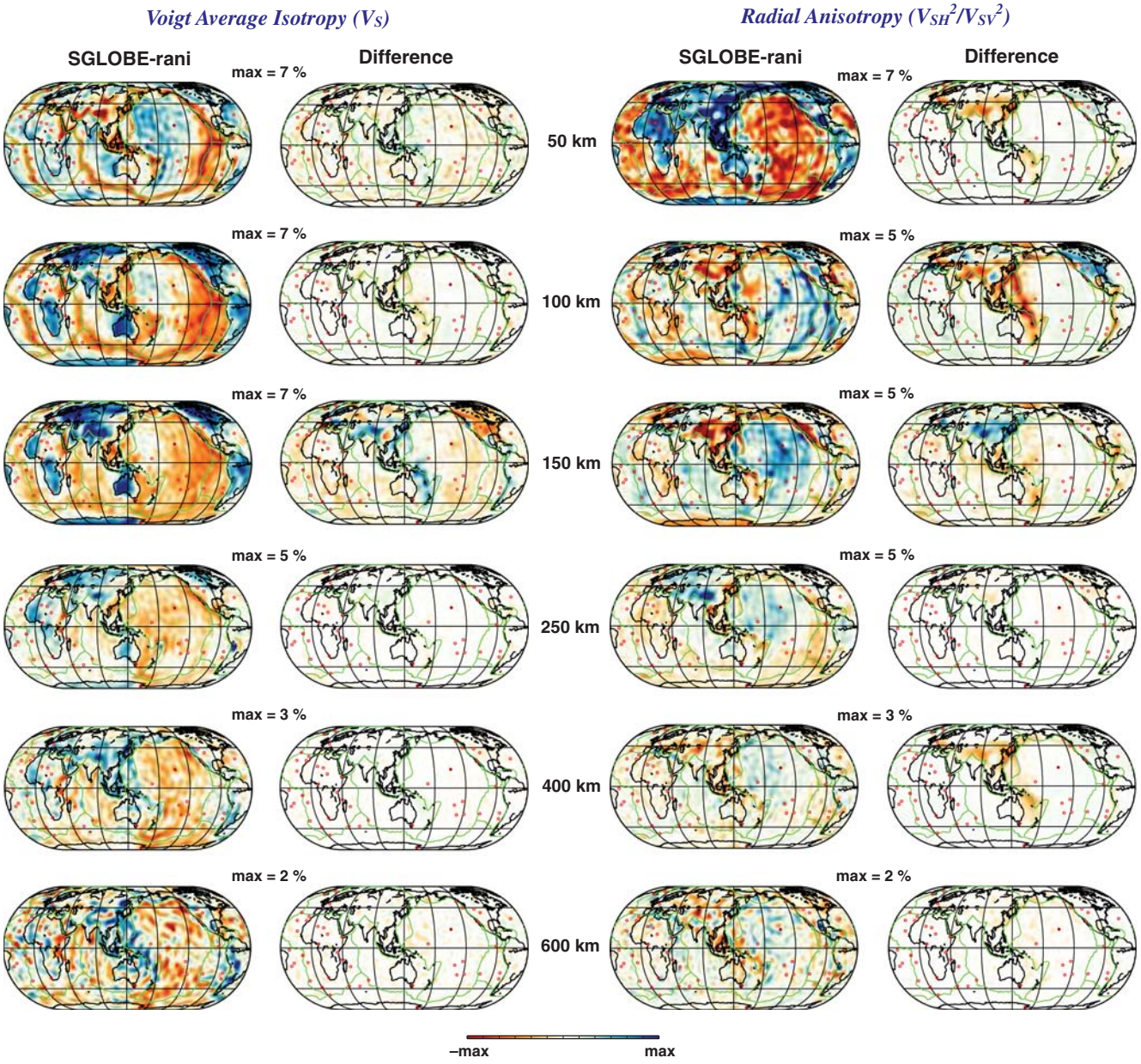

Figure 5. Depth slices of perturbations from SGLOBE-rani and differences between models from tomographic inversions with and without crustal perturbations (SGLOBE-rani—the model obtained by inverting only for Voigt average isotropy and radial anisotropy) for Voigt average isotropy and radial anisotropy, respectively. The range of model amplitude variations is shown at the top of each depth slice.

and Love waves in the period range of $T \sim 18$–145 s and $T \sim 25$–145 s, respectively (Ritzwoller *et al.*, 2002). LITHO1.0 is a 1° tessellated model of the crust and uppermost mantle, which was built by constructing an appropriate starting model and by perturbing it to fit surface-wave dispersion curves (phase and group velocity with the 25–200 s period range). The starting model is the combination of CRUST1.0 for the crust and the LLNL-G3D model (Simmons *et al.*, 2012) for the upper mantle. As shown in Figure 6, SGLOBE-rani has lower resolution than other high-resolution models because it was built using spherical harmonic basis functions up to degree 35. We recall that our main purpose is not to build a new high-resolution global crustal model, but rather to constrain Moho perturbations that help better infer mantle anisotropy in a self-consistent way. Hence, the comparisons in this section serve as a consistency check between the various crustal models to verify the reasonableness of our crustal model and to further validate our modeling approach. A detailed comparative assessment of the quality of the various crustal models is beyond the scope of this study.

Figure 6 shows some discrepancies between the four models as well as some common features. SGLOBE-rani shows large Moho depth perturbations mainly in oceanic crusts in the southwestern and western Pacific. Anomalies with small amplitudes in oceanic crusts are probably not meaningful, and

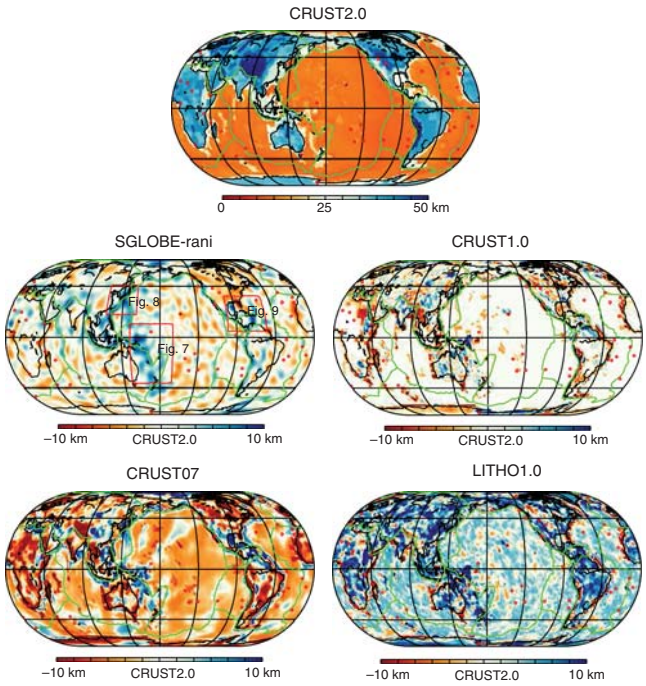

Figure 6. Crustal thickness perturbations from SGLOBE-rani (Chang *et al.*, 2015), CRUST1.0 (Laske *et al.*, 2013), CRUST07 (Meier *et al.*, 2007), and LITHO1.0 (Pasyanos *et al.*, 2014) with respect to CRUST2.0 (Bassin *et al.*, 2000). Crustal thickness distributions from CRUST2.0 are shown on the top panel. The regions presented in Figures 7–9 are indicated by red rectangles.

are probably related to the spherical harmonics parameterization used in the inversions. CRUST1.0 seems to exhibit large crustal thickness variations mostly in continental crusts and small perturbations in oceanic crusts. CRUST07 shows large variations in crustal thickness, with strong lateral changes. It exhibits very thin oceanic crusts (e.g., ∼4 km thinner oceanic crust than CRUST2.0 away from subduction zones) and it shows thicker crust along the subduction zones in the western Pacific as in SGLOBE-rani. In contrast, LITHO1.0 shows overall thicker crust than the other models (e.g., ∼5 km thicker oceanic crust than CRUST2.0). The differences between CRUST07 and LITHO1.0 are somewhat surprising given that both models are based on surface-wave dispersion data. This discrepancy may be due to the different period range of data used and to different modeling approaches.

To assess these different features in the crustal models, we need to carry out comparisons with reliable data sets. Thus, we compare the four models with high-resolution Moho depth measurements from seismic refraction surveys and receiver functions for oceanic crust. As explained previously, unlike CRUST07 and LITHO1.0, CRUST1.0 and CRUST2.0 are based on large compilations of geophysical information, including seismic refraction data and receiver function studies. However, at present the full list of data sources and references used in the construction of CRUST1.0 and CRUST2.0 has not been made publicly available, and thus it is not entirely clear whether the refraction and receiver function data used in this study are included in CRUST1.0 or CRUST2.0. Hence, our various comparisons between crustal models and refraction data may not be entirely independent.

Continental crustal structure can be very heterogeneous due to complex orogenic activities, including, for example, partial melting due to continental collision (e.g., Owens and Zandt, 1997), making it potentially more difficult to model using global approaches. Because of the strong trade-off between crustal thickness and velocity (Lebedev *et al.*, 2013), in the construction of SGLOBE-rani we only model crustal thickness and keep the crustal velocity fixed to that of CRUST2.0. Hence, the retrieved crustal thickness perturbations may be contaminated by uncorrected crustal velocity. This issue should be less severe for oceanic crustal structure, which is more homogeneous than continental crust. Thus, we focus on three areas where large oceanic Moho depth perturbations are observed in SGLOBE-rani: subduction zones in the southwestern Pacific (Fig. 7), in the western Pacific (Fig. 8), and in the Caribbean Sea (Fig. 9).

For the southwestern Pacific region, CRUST2.0 and refraction survey data are overall consistent with each other except for the Ontong Java plateau, where thicker crust is found by the refraction survey data (Furumoto *et al.*, 1970; Gladczenko *et al.*, 1997; top left panel in Fig. 7). This inconsistency suggests that CRUST2.0 does not include the refraction data we collected for the Ontong Java plateau. Interestingly, the other four crustal models show thicker crust beneath the Ontong Java plateau, which is consistent with each other and with the refraction survey data. The Ontong Java plateau is expected to have thicker than average oceanic crust due to a massive magmatic eruption by a mantle plume (Tarduno *et al.*, 1991). On the other hand, most of the models depict thin crust beneath the north Fiji basin, where ridges are active (orange lines in Fig. 7). Furthermore, in the west of New Zealand and around the New Hebrides trench, all four models show thicker crust than CRUST2.0, despite differences in the detailed structures in each model. Thus, overall, we observe that SGLOBE-rani is generally consistent with the large-scale features in the other crustal models, showing similar perturbations from CRUST2.0.

We estimate the root mean square (rms) misfit of Moho depths in each model with respect to values from the seismic refraction survey data assembled (59 points in Table 1; Furumoto *et al.*, 1970; Shor *et al.*, 1971; Gladczenko *et al.*, 1997), using the following equation:

$$\mathrm{rms} = \sqrt{\frac{\sum_{i=1}^{n}(C_m - C_r)^2}{n-1}}, \qquad (1)$$

in which n is the total number of data, C_m and C_r are Moho depth from the five crustal models and refraction surveys, respectively. The results for CRUST1.0, CRUST2.0, CRUST07, LITHO1.0, and SGLOBE-rani are 4.97, 7.48, 6.14, 6.52, and 5.45 km, respectively. SGLOBE-rani shows quite good agreement with results from refraction surveys despite its low resolution.

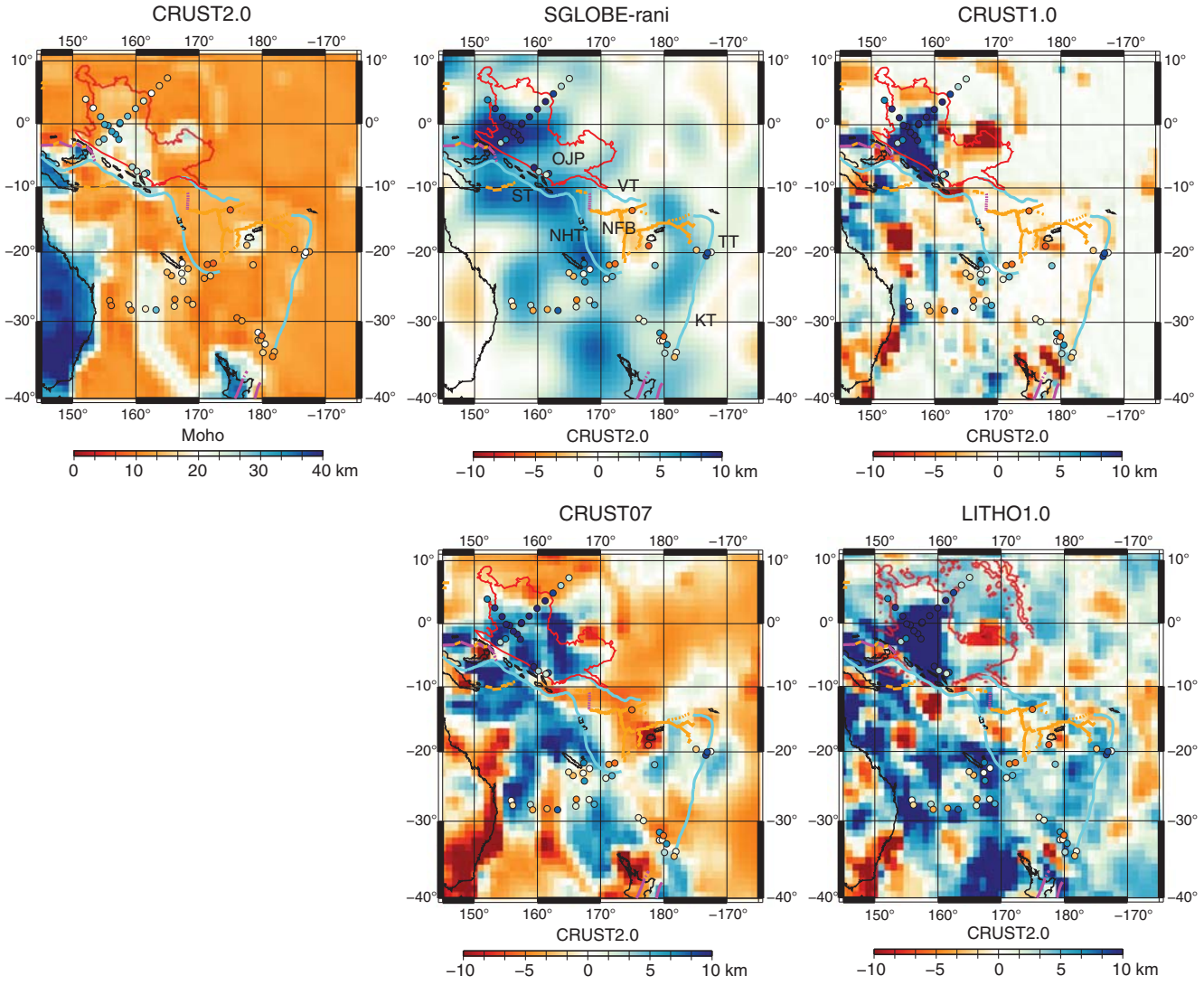

Figure 7. Crustal thickness perturbations from SGLOBE-rani, CRUST1.0, CRUST07, and LITHO1.0 with respect to CRUST2.0 for the southwestern Pacific. Crustal thickness distributions from CRUST2.0 are presented in the left panel. Crustal thickness perturbations from refraction surveys are superposed on the maps as circles with the same color scale as in the crustal thickness perturbation maps for SGLOBE-rani, CRUST1.0, CRUST07, and LITHO1.0 and in the map for CRUST2.0. The Ontong Java plateau is enclosed by red solid lines based on bathymetry of 4000 m. Plate boundaries from Bird (2003) are depicted by colored lines: orange, magenta, and cyan lines represent ridges, transform faults, and trenches, respectively. KT, Kermadec trench; NFB, north Fiji basin; NHT, New Hebrides trench; OJP, Ontong Java plateau; ST, Solomon trench; TT, Tonga trench; VT, Vitiaz trench.

In Figure 8, we compare the various crustal models for the western Pacific. We collected seismic refraction survey data across trenches in Japan (43 points in Table 2) reported by Iwasaki *et al.* (1989, 1990), Hetland and Wu (2001), Kodaira *et al.* (2002), Takahashi *et al.* (2004, 2009), and Nakamura (2014). For this region, the Moho depths from CRUST2.0 and from refraction data seem to be generally consistent. The main discrepancies seem to occur near trenches, where thicker crust is found by the refraction data within short ranges. Thicker crust than CRUST2.0 along the subduction zones is also found in the other crustal models except CRUST1.0, but this feature is probably smeared out to wide areas due to limited resolution. The misfits of the crustal thickness models with respect to the refraction survey data (equation 1) are 9.86, 10.01, 9.47, 8.82, and 8.99 km for CRUST1.0, CRUST2.0, CRUST07, LITHO1.0, and SGLOBE-rani, respectively. Overall, the Moho depths from SGLOBE-rani fit the results from refraction data as well or even slightly better than other models, notably by showing thick crust near the trenches. Nevertheless, for all models the fit is poorer than for the southwestern Pacific (Fig. 7). This is probably due to the coarse grids used in the models' construction, which do not capture the dramatic variations in crustal thickness across the trenches shown by the refraction data.

In Figure 9, we compare the various crustal models for the Caribbean Sea and the Gulf of Mexico. We collected 42 points (Table 3) of refraction survey and receiver function data from Ibrahim and Uchupi (1982), Niu *et al.* (2007),

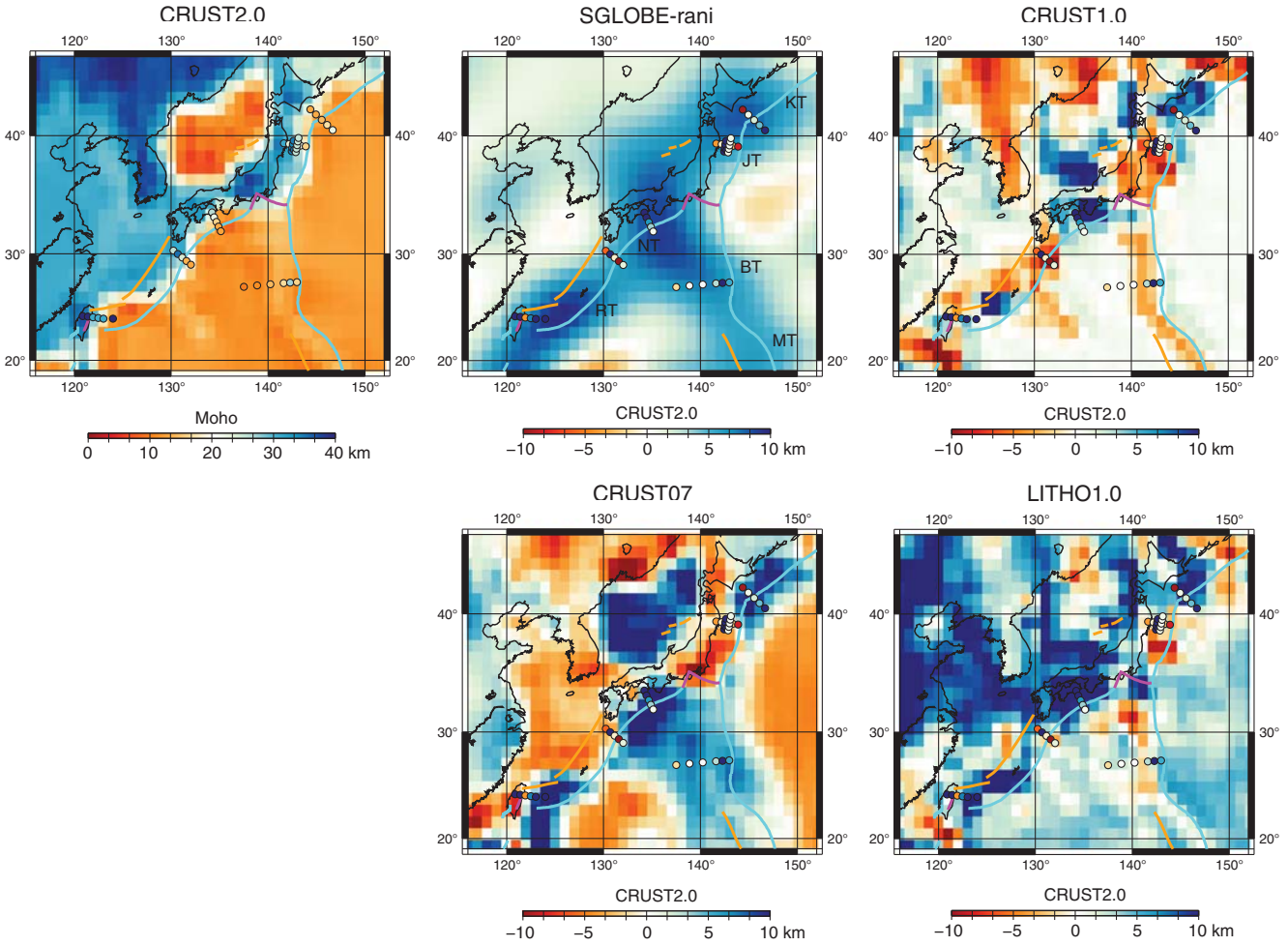

Figure 8. Crustal thickness perturbations from SGLOBE-rani, CRUST1.0, CRUST07, and LITHO1.0 with respect to CRUST2.0 for the western Pacific. The crustal thickness distribution from CRUST2.0 is shown at the left panel. Crustal thickness perturbations from refraction surveys are superimposed on the maps as circles with the same color scale as the crustal thickness perturbation maps for SGLOBE-rani, CRUST1.0, CRUST07, and LITHO1.0, and depth map for CRUST2.0. Plate boundaries from Bird (2003) are depicted by colored lines: orange, magenta, and cyan lines represent ridges, transform faults, and trenches, respectively. BT, Bonin trench; JT, Japan trench; KT, Kuril trench; MT, Mariana trench; NT, Nankai trough; RT, Ryukyu trench.

Guedez (2007), Christeson *et al.* (2008, 2014), Clark *et al.* (2008), and Magnani *et al.* (2009). In the comparison between CRUST2.0 and the collected Moho data, two main discrepancies are observed beneath the Gulf of Mexico and the southern Caribbean deformed belt (SCDB). In the Gulf of Mexico, the refraction data indicate thinner crust than CRUST2.0, whereas in the SCDB a rapid variation is observed from thicker to thinner crust. Interestingly, all the crustal models except CRUST1.0 show thicker crust than CRUST2.0 beneath the Gulf of Mexico. This is possibly because while CRUST1.0 may include the refraction survey data used in these comparisons, the other models are built using surface-wave data. The very low crustal velocity due to a thick sedimentary layer in the Gulf of Mexico may obscure the proper estimation of its Moho's depth using surface waves. Indeed, an unconstrained low-velocity layer may cause apparent thicker crust in the models to fit the surface-wave data. On the other hand, the rapid variation in Moho's depth in the SCDB is generally shown in all the four models, but CRUST1.0 does not match well the thicker crust in this region. The rms misfit (equation 1) for CRUST1.0, CRUST2.0, CRUST07, LITHO1.0, and SGLOBE-rani are 11.45, 11.03, 13.23, 12.84, and 10.81 km, respectively.

Based on the aforementioned cases, we conclude that, despite their lower resolution, the crustal thickness perturbations associated with SGLOBE-rani match Moho depths in the regions investigated as well as other recent global crustal models, and show a better rms misfit than its initial crustal model, CRUST2.0. These comparisons suggest that SGLOBE-rani provides reliable information on oceanic crustal thickness, highlighting the performance of our strategy of joint inversions for crustal thickness and mantle isotropic and anisotropic structures.

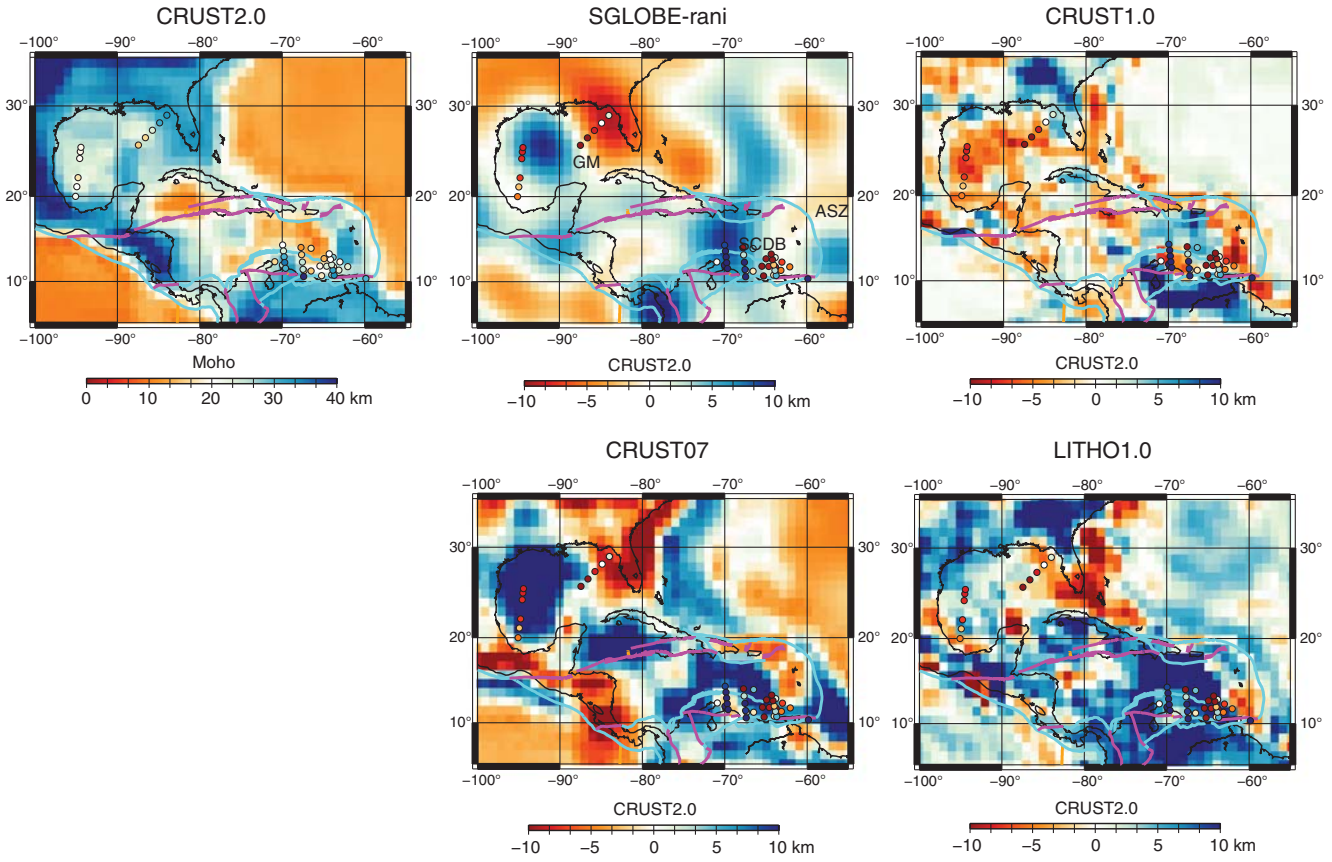

Figure 9. Crustal thickness perturbations from SGLOBE-rani, CRUST1.0, CRUST07, and LITHO1.0 with respect to CRUST2.0 for the Caribbean Sea and the Gulf of Mexico. The crustal thickness distribution from CRUST2.0 is shown at the left panel. Crustal thickness perturbations from refraction surveys are superposed on the maps as circles with the same color scale as the crustal thickness perturbation maps for SGLOBE-rani, CRUST1.0, CRUST07, and LITHO1.0, and depth map for CRUST2.0. Plate boundaries from Bird (2003) are depicted by colored lines: orange, magenta, and cyan lines represent ridges, transform faults, and trenches, respectively. ASZ, Antilles subduction zone; GM, the Gulf of Mexico; SCDB, southern Caribbean deformed belt.

Discussion and Conclusions

In this study, we conducted a series of real data and synthetic resolution tests to understand the importance of simultaneously inverting for crustal thickness perturbations and for mantle isotropic and radially anisotropic structure in global tomography. Because unaccounted crustal structure influences the mapping of radial anisotropy in the Earth's mantle significantly (Ferreira *et al.*, 2010; Xing and Beghein, 2015), we included crustal thickness perturbations as model parameters in global tomographic inversions to better account for crustal effects (Chang *et al.*, 2014, 2015).

First, our tests showed that short-period group velocity data are essential to constrain crustal structure, and that group velocity data with wave periods down to at least $T \sim 20$ s are necessary to properly image thin oceanic crust. Second, we demonstrated that uncorrected crustal structure has a strong influence on retrieved mantle radial anisotropy structure, notably at 100–150 km depth. Therefore, adding crustal thickness perturbations as model parameters to the tomographic inversions reduces the distortion of the retrieved radial anisotropy by uncorrected crustal structure, whose effects can persist down to the mantle transition zone. There have been several attempts to adopt group velocity data in global tomography studies (e.g., Shapiro and Ritzwoller, 2002; Lekić and Romanowicz, 2011; French *et al.*, 2013; French and Romanowicz, 2014). However, most previous studies used group velocity data down to $T \sim 25$ s to constrain crustal structure, which potentially limits the robustness of the retrieved mantle anisotropy structure. To understand why it is necessary to use data with wave periods shorter than 25 s, it is useful to examine the sensitivity kernels of Rayleigh- and Love-wave group velocity data (Fig. 10), which are quite distinct, especially for crustal depths (< 25 km). While group velocity measurements of Love waves are strongly sensitive to the crust, $T \sim 25$ s Rayleigh waves have little sensitivity to structure at crustal depths. On the other hand, shorter-period Rayleigh waves (less than 25 s) show stronger sensitivity to the crust. Unresolved crustal anisotropy due to the big differences in sensitivities of $T \sim 25$ s Rayleigh and Love waves may be responsible for the distortion of the retrieved mantle anisotropy. Because Rayleigh waves dominate the group velocity data set used in our inversions, it becomes clear

Table 1
Moho Measurements for the Southwestern Pacific

Longitude (°)	Latitude (°)	Moho Depth (km)	Reference
159.4167	−6.8667	26.7	Furumoto *et al.* (1970)
160.1667	−7.5333	25.0	
161.7333	−7.8083	29.9	
161.3667	−8.0000	25.5	
168.2500	−22.4833	13.9	Shor *et al.* (1971)
167.3333	−21.8667	20.2	
171.3167	−21.6500	9.2	
172.2500	−21.6833	8.0	
171.8000	−23.5333	15.2	
170.8333	−23.9000	11.8	
167.4333	−24.3000	21.1	
167.2500	−23.1500	21.6	
165.6333	−23.5167	12.9	
164.9500	−23.0000	14.3	
155.8667	−27.1000	11.1	
156.1000	−27.7833	9.7	
158.9000	−27.6667	17.5	
159.2500	−28.4000	10.9	
161.5333	−28.2500	18.0	
163.1833	−28.4167	29.0	
166.0833	−27.8833	16.9	
166.1667	−26.9333	10.4	
168.1833	−26.9667	11.6	
169.0000	−27.6167	15.4	
176.0000	−29.5000	10.0	
176.7667	−29.9167	12.6	
179.3333	−31.5000	20.0	
179.3333	−32.5667	14.0	
179.7500	−32.5500	13.0	
179.9333	−31.9500	8.7	
−179.550	−33.0667	19.1	
−179.8833	−34.200	16.2	
−178.0833	−34.0833	14.1	
−178.350	−34.7000	10.4	
174.9333	−13.6000	8.1	
177.5667	−18.9833	15.2	
178.5500	−21.9167	14.7	
−174.900	−19.6167	11.9	
−172.550	−19.9500	12.3	
−173.3333	−20.5000	20.4	
−173.1167	−20.0333	20.1	
157.3167	−2.4667	31.25	Gladczenko *et al.* (1997)
156.8000	−1.6833	31.88	
155.6135	−0.2787	31.25	
155.0417	−0.1000	30.63	
154.4273	1.1260	28.75	
153.2399	2.5302	20.63	
152.0500	3.9333	18.13	
154.1333	−2.9333	25.0	
154.9500	−2.4333	28.75	
156.2023	−1.2170	31.25	
157.4534	−0.0001	32.50	
157.5000	0.1667	31.25	
158.7046	1.2167	28.75	
159.9569	2.4330	26.25	
161.2115	3.6482	23.75	
162.4694	4.8616	20.00	
163.7319	6.0726	14.38	
165.0000	7.2807	13.75	

Table 2
Moho Measurements for the Western Pacific

Longitude (°)	Latitude (°)	Moho Depth (km)	Reference
144.3704	42.0556	13.17	Iwasaki *et al.* (1989)
144.9552	41.6571	13.17	
145.5327	41.2557	14.27	
146.1032	40.8514	16.83	
146.6667	40.4444	22.32	
130.2308	30.2889	25.60	Iwasaki *et al.* (1990)
130.6838	29.9746	35.20	
131.1339	29.6588	24.00	
131.5812	29.3415	13.60	
132.0257	29.0227	12.80	
120.8724	24.2581	56.88	Hetland and Wu (2001)
121.4051	24.1963	55.13	
121.9373	24.1327	30.63	
122.4690	24.0673	30.10	
123.0000	24.0000	30.63	
134.2069	33.6429	25.93	Kodaira *et al.* (2002)
134.4386	33.2328	22.22	
134.6680	32.8222	15.74	
134.8954	32.4113	12.96	
135.1207	32.0000	12.50	
141.6212	39.3929	30.75	Takahashi *et al.* (2004)
142.1909	39.3345	23.25	
142.7596	39.2734	20.63	
143.0437	39.2418	26.25	
143.3273	39.2095	21.75	
143.8940	39.1429	15.75	
142.4394	38.7500	34.50	
142.5030	39.0328	34.13	
142.5672	39.3156	33.75	
142.6318	39.5983	34.50	
142.6970	38.8801	34.50	
142.8636	38.6786	25.13	
142.9310	38.9643	25.13	
142.9989	39.2500	24.75	
143.0673	39.5356	24.75	
143.1363	39.8212	25.13	
137.5000	26.9800	9.80	Takahashi *et al.* (2009)
138.8646	27.1096	11.02	
140.2321	27.2259	14.08	
141.6024	27.3289	16.53	
142.2884	27.3754	26.94	
142.9750	27.4186	15.92	
124.0000	24.0000	42.67	Nakamura (2014)

that $T \leq 20$ s group velocity data are needed to properly constrain crustal thickness and hence to reduce the contamination of unresolved crustal features into the retrieved mantle anisotropy.

Recently, Xing and Beghein (2015) assessed the importance of crustal corrections in radially anisotropic tomography using a Bayesian approach, whereby they compare model uncertainty with the influence of various crustal corrections. They show that retrieved radial anisotropy is more sensitive to crustal corrections than isotropic structure, especially for 100–150 km depth, which is consistent with this and previous studies (e.g., Ferreira *et al.*, 2010). They find that crustal effects are larger than model uncertainty beneath continental crust such as Tibet, North America, and South

Table 3
Moho Measurements for the Caribbean Sea and the Gulf of Mexico

Longitude (°)	Latitude (°)	Moho Depth (km)	Reference
−95.0700	20.0000	21.18	Ibrahim and Uchupi (1982)
−94.9300	21.1100	20.00	
−94.7800	22.1500	17.25	
−94.5700	24.3000	19.61	
−94.4900	25.0400	19.22	
−94.4200	25.5300	19.22	
−63.1320	11.3552	23.2	Niu *et al.* (2007)
−63.9925	10.7858	27.3	
−64.5977	11.8216	24.0	
−69.9705	11.9550	26.4	
−70.9023	12.3585	16.2	
−65.4180	11.8499	19.2	
−63.7699	11.7515	18.5	
−66.4910	13.9497	16.8	
−65.2200	10.6796	18.0	
−66.5009	11.2493	15.1	
−67.3496	11.2707	16.2	
−64.9313	12.7209	14.0	
−69.9400	14.3300	20.05	Guedez (2007)
−69.8568	13.6425	23.97	
−69.7741	12.9551	29.84	
−69.6918	12.2675	34.73	
−69.6100	11.5800	29.84	
−59.8500	10.3300	29.81	Christeson *et al.* (2008)
−62.0600	11.7600	23.33	
−62.9918	12.3238	19.44	
−63.8200	12.8800	27.87	
−63.6900	10.7200	33.16	Clark *et al.* (2008)
−63.8439	11.3601	31.63	
−63.9985	12.0002	23.98	
−64.1539	12.6401	19.90	
−64.3100	13.2800	19.90	
−67.7300	14.0600	11.58	Magnani *et al.* (2009)
−67.6441	13.1900	15.26	
−67.5589	12.3201	25.26	
−67.4742	11.4501	25.26	
−67.3900	10.5800	44.74	
−84.0000	29.0000	32.73	Christeson *et al.* (2014)
−84.8817	28.2006	30.91	
−85.7502	27.3956	23.64	
−86.6061	26.5853	16.36	
−87.4500	25.7700	15.45	

America, which are also regions identified in our study as having strong crustal effects. However, their study probably comprises conservative bounds of crustal effects, because they only use fundamental and higher-mode phase velocity data down to a wave period of 35 s. As shown before, this period range seems inadequate to resolve crustal structure. Therefore, there are likely wider areas of significant crustal effects beyond model uncertainty when shorter-period phase/group velocity data are used such as along the subduction zones in the western Pacific. Because it is quite challenging to fully quantify model uncertainty, we do not know whether our estimated Moho perturbations are beyond model uncertainty. Nevertheless, we studied the effect of regularization on the retrieved Moho perturbations (Fig. 11). The various

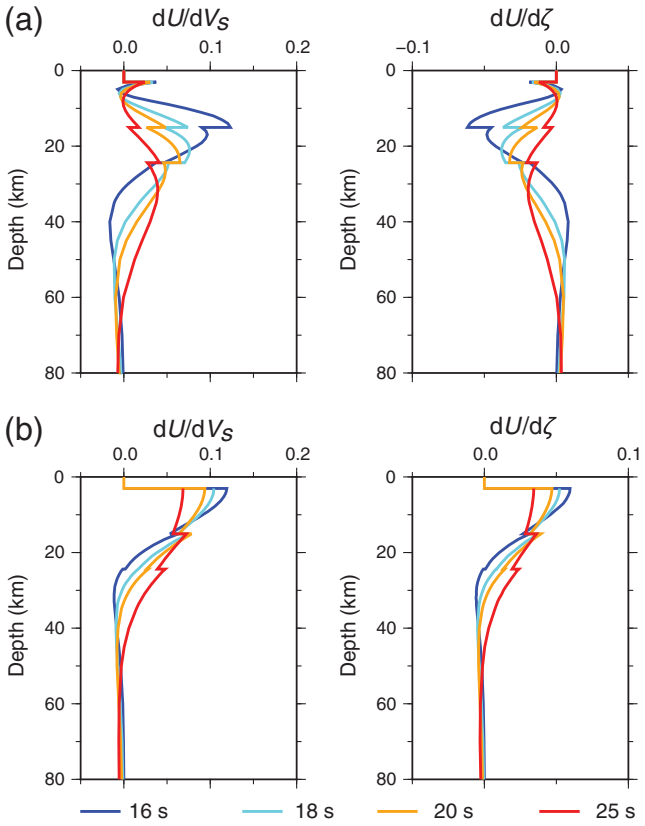

Figure 10. Sensitivity kernels of group velocity with respect to isotropy and anisotropy for PREM. (a) Sensitivity kernels of Rayleigh wave. (b) Sensitivity kernels of Love wave.

models considered with different levels of regularization show very similar features of thick crusts along subduction zones, which is the most peculiar feature in the Moho perturbations associated with SGLOBE-rani. This suggests that the retrieved thick crust along subduction zones is a robust feature beyond errors associated with regularization.

To further verify our approach and the crustal thickness perturbations from CRUST2.0 associated with SGLOBE-rani, we then compared the corresponding Moho depths with other global crustal models (CRUST1.0, CRUST07, and LITHO1.0) and with results from seismic refraction survey data and receiver function data obtained across trenches in the southwestern and western Pacific and the Caribbean Sea. Despite having lower resolution, SGLOBE-rani shows good consistency with the previous crustal models and with results from refraction survey data and receiver function data. This suggests that SGLOBE-rani properly resolves Moho depths (notably in oceanic regions along subduction zones), and thus reduces the contamination of unresolved crustal features into the retrieved mantle anisotropy. The crustal thickness results may depend on the choice of the initial model, because we linearize the problem after applying nonlinear crustal corrections to the data based on the initial model. Therefore, to avoid biases in the results, it is important to choose a proper initial crustal model providing a good initial description of crustal properties.

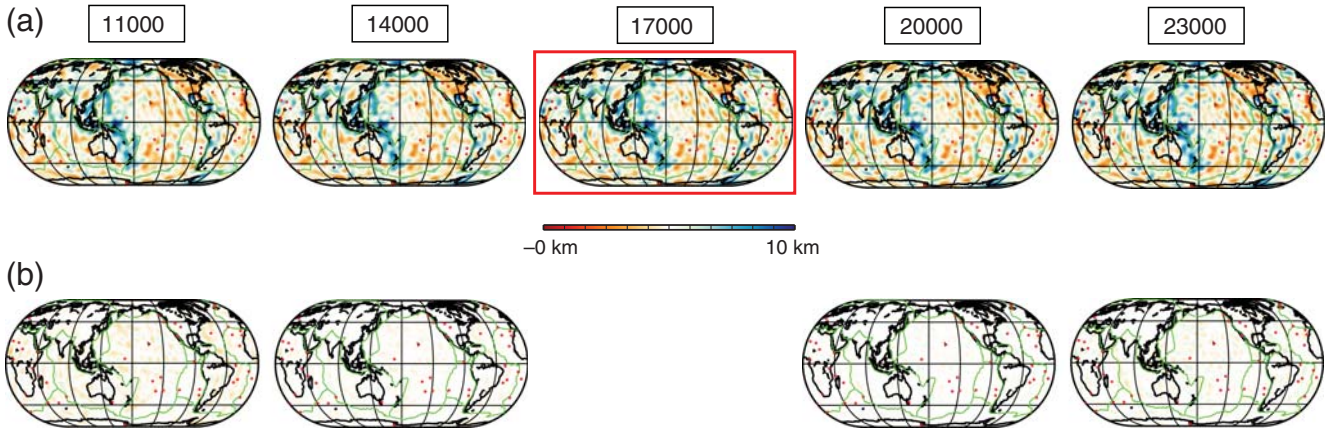

Figure 11. (a) Moho perturbations obtained from successive real data inversions only varying the level of regularization applied. The corresponding effective number of model parameters is shown at the top of each map. SGLOBE-rani is enclosed by a red rectangle. (b) Differences between each model and SGLOBE-rani.

Data and Resources

Seismograms used in this study were collected from the Incorporated Research Institutions for Seismology (IRIS) Data Management Center. All figures were created using the Generic Mapping Tools v.4.5.11 (www.soest.hawaii.edu/gmt, last accessed August 2015; Wessel and Smith, 1998).

Acknowledgments

This research was initially supported by the Leverhulme Trust (Project F/00204/AS), followed by support of the National Environmental Research Council (NERC) Project NE/K005669/1, Basic Science Research Program through the National Research Foundation of Korea (NRF) funded by the Ministry of Education (NRF-2014R1A1A2056925), the Korea Meteorological Administration Research and Development Program under Grant KMIPA 2015-7030, and 2014 Research Grant from Kangwon National University (Number 120141511). A. M. G. F. acknowledges discussions and mobility supported by the European Cooperation in Science and Technology (COST) Action ES1401-TIDES.

References

Bassin, C., G. Laske, and G. Masters (2000). The current limits of resolution for surface wave tomography in North America, *Eos Trans. AGU* **81,** Abstract S12A–03.

Bird, P. (2003). An updated digital model of plate boundaries, *Geochem. Geophys. Geosyst.* **4,** 1027, doi: 10.1029/2001GC000252.

Bozdağ, E., and J. Trampert (2008). On crustal corrections in surface wave tomography, *Geophys. J. Int.* **172,** 1066–1082.

Chang, S.-J., A. M. G. Ferreira, and M. Faccenda (2016). Upper- and mid-mantle interaction between the Samoan plume and the Tonga-Kermadec slabs, *Nature Comm.* **7,** doi: 10.1038/ncomms10799.

Chang, S.-J., A. M. G. Ferreira, J. Ritsema, H. J. van Heijst, and J. H. Woodhouse (2014). Global radially anisotropic mantle structure from multiple datasets: A review, current challenges, and outlook, *Tectonophysics* **617,** 1–19.

Chang, S.-J., A. M. G. Ferreira, J. Ritsema, H. J. van Heijst, and J. H. Woodhouse (2015). Joint inversion for global isotropic and radially anisotropic mantle structure including crustal thickness perturbations, *J. Geophys. Res.* **120,** 4278–4300, doi: 10.1002/2014JB011824.

Chen, M., F. Niu, Q. Liu, J. Tromp, and X. Zheng (2015). Multiparameter adjoint tomography of the crust and upper mantle beneath East Asia: 1. Model construction and comparisons, *J. Geophys. Res.* **120,** no. 3, 1762–1786, doi: 10.1002/2014JB011638.

Christeson, G. L., P. Mann, A. Escalona, and T. J. Aitken (2008). Crustal structure of the Caribbean–northeastern South America arc-continent collision zone, *J. Geophys. Res.* **113,** no. B08104, doi: 10.1029/2007JB005373.

Christeson, G. L., H. J. A. Van Avendonk, I. O. Norton, J. W. Snedden, D. R. Eddy, G. D. Karner, and C. A. Johnson (2014). Deep crustal structure in the eastern Gulf of Mexico, *J. Geophys. Res.* **119,** 6782–6801, doi: 10.1002/2014JB011045.

Clark, S. A., C. A. Zelt, M. B. Magnani, and A. Levander (2008). Characterizing the Caribbean–South American plate boundary at 64° W using wide-angle seismic data. *J. Geophys. Res.* **113,** no. B07401, doi: 10.1029/2007JB005329.

Dziewoński, A. M., and D. L. Anderson (1981). Preliminary reference Earth model, *Phys. Earth Planet. In.* **25,** 297–356.

Ekström, G., and A. M. Dziewoński (1998). The unique anisotropy of the Pacific upper mantle, *Nature* **394,** 168–172.

Ferreira, A. M. G., J. H. Woodhouse, K. Visser, and J. Trampert (2010). On the robustness of global radially anisotropic surface wave tomography, *J. Geophys. Res.* **115,** no. B04313, doi: 10.1029/2009JB006716.

Fichtner, A., B. L. N. Kennett, H. Igel, and H.-P. Bunge (2009). Full seismic waveform tomography for upper-mantle structure in the Australasian region using adjoint methods, *Geophys. J. Int.* **179,** 1703–1725.

French, S., V. Lekić, and B. Romanowicz (2013). Waveform tomography reveals channeled flow at the base of the oceanic asthenosphere, *Science* **342,** 227–230.

French, S. W., and B. Romanowicz (2014). Whole-mantle radially anisotropic shear velocity structure from spectral-element waveform tomography, *Geophys. J. Int.* **199,** 1303–1327.

Furumoto, A. S., D. M. Hussong, J. F. Campbell, G. H. Sutton, A. Malahoff, J. C. Rose, and G. P. Woollard (1970). Crustal and upper mantle structure of the Solomon Islands as revealed by seismic refraction survey of November–December 1966, *Pac. Sci.* **24,** 315–332.

Gladczenko, T. P., M. F. Coffin, and O. Eldholm (1997). Crustal structure of the Ontong Java plateau: Modeling of new gravity and existing seismic data, *J. Geophys. Res.* **102,** no. B10, 22,711–22,729.

Gu, Y. J., A. L. Lerner-Lam, A. M. Dziewoński, and G. Ekström (2005). Deep structure and seismic anisotropy beneath the East Pacific Rise, *Earth Planet. Sci. Lett.* **232,** 259–272.

Guedez, M. (2007). Crustal structure across the Caribbean–South American plate boundary at 70°W: Results from seismic refraction and reflection data, *M.S. Thesis*, Rice University, Houston, Texas.

Hetland, E. A., and F. T. Wu (2001). Crustal structure at the intersection of the Ryukyu trench with the arc-continent collision in Taiwan: Results from an offshore–onshore seismic experiment, *Terr. Atmos. Ocean. Sci.* **12,** 231–248.

Ibrahim, A.-B. K., and E. Uchupi (1982). Continental oceanic crustal transition in the Gulf coast geosyncline, *Am. Assoc. Petroleum Geologists Mem.*, Vol. **34,** 155–165.

Iwasaki, T., N. Hirata, T. Kanazawa, J. Melles, K. Suyehiro, T. Urabe, L. Moller, J. Makris, and H. Shimamura (1990). Crustal and upper mantle structure in the Ryukyu Island arc deduced from deep seismic sounding, *Geophys. J. Int.* **192,** 631–651.

Iwasaki, T., H. Shiobara, A. Nishizawa, T. Kanazawa, K. Suyehiro, N. Hirata, T. Urabe, and H. Shimamura (1989). A detailed subduction structure in the Kuril trench deduced from ocean bottom seismographic refraction studies, *Tectonophysics* **165,** 315–336.

Karato, S.-I., H. Jung, I. Katayama, and P. Skemer (2008). Geodynamic significance of seismic anisotropy of the upper mantle: New insights from laboratory studies, *Annu. Rev. Earth Planet. Sci.* **36,** 59–95.

Kodaira, S., E. Kurashimo, J.-O. Park, N. Takahashi, A. Nakanishi, S. Miura, T. Iwasaki, N. Hirata, K. Ito, and Y. Kaneda (2002). Structural factors controlling the rupture process of a megathrust earthquake at the Nankai trough seismogenic zone, *Geophys. J. Int.* **149,** 815–835.

Kustowski, B., A. M. Dziewonski, and G. Ekstrom (2007). Nonlinear crustal corrections for normal-mode seismograms, *Bull. Seismol. Soc. Am.* **97,** 1756–1762.

Laske, G., G. Masters, Z. Ma, and M. Pasyanos (2013). Update on CRUST1.0—A 1-degree global model of Earth's crust, *Geophys. Res. Abstr.* **15,** Abstract EGU 2013–2658.

Lebedev, S., J. M.-C. Adam, and T. Meier (2013). Mapping the Moho with seismic surface waves: A review, resolution analysis, and recommended inversion strategies, *Tectonophysics* **609,** 377–394, doi: 10.1016/j.tecto.2012.12.030.

Lekić, V., and B. Romanowicz (2011). Inferring upper-mantle structure by full waveform tomography with the spectral element method, *Geophys. J. Int.* **185,** 799–831.

Magnani, M. B., C. A. Zelt, A. Levander, and M. Schmitz (2009). Crustal structure of the South American–Caribbean plate boundary at 67° W from controlled source seismic data, *J. Geophys. Res.* **114,** no. B02312, doi: 10.1029/2008JB005817.

Marone, F., and B. Romanowicz (2007). Non-linear crustal corrections in high-resolution regional waveform seismic tomography, *Geophys. J. Int.* **170,** 460–467.

Meier, U., A. Curtis, and J. Trampert (2007). Fully nonlinear inversion of fundamental mode surface waves for a global crustal model, *Geophys. Res. Lett.* **34,** L16304, doi: 10.1029/2007GL030989.

Montagner, J., and N. Jobert (1988). Vectorial tomography—II. Application to the Indian Ocean, *Geophys. J. Int.* **94,** 309–344.

Mooney, W. D., G. Laske, and G. Masters (1998). CRUST5.1: A global crustal model at 5° × 5°, *J. Geophys. Res.* **103,** 727–747.

Nakamura, M. (2014). Seismic structure of subducted oceanic crust near the slow-earthquake source region in the southern Ryukyu arc, *Earth Planets Space* **66,** no. 96, doi: 10.1186/1880-5981-66-96.

Niu, F., T. Bravo, G. Pavlis, F. Vernon, H. Rendon, M. Bezeda, and A. Levander (2007). Receiver function study of the crustal structure of the southeastern Caribbean plate boundary and Venezuela, *J. Geophys. Res.* **112,** no. B11308, doi: 10.1029/2006JB004802.

Owens, T. J., and G. Zandt (1997). Implications of crustal property variations for models of Tibetan plateau evolution, *Nature* **387,** 37–43.

Parisi, L., and A. M. G. Ferreira (2016). Empirical assessment of the validity limits of the surface wave full ray theory using realistic 3-D Earth models, *Geophys. J. Int.* **205,** 146–159, doi: 10.1093/gji/ggw005.

Pasyanos, M. E., G. Masters, G. Laske, and Z. Ma (2014). LITHO1.0: An updated crust and lithospheric model of the Earth, *J. Geophys. Res.* **119,** 2153–2173, doi: 10.1002/2013JB010626.

Ritsema, J., H. J. van Heijst, J. H. Woodhouse, and A. Deuss (2009). Long-period body wave traveltimes throughout the crust: Implication for crustal corrections and seismic tomography, *Geophys. J. Int.* **179,** 1255–1261.

Ritzwoller, M. H., and A. L. Levshin (1998). Eurasian surface wave tomography: Group velocities, *J. Geophys. Res.* **103,** 4839–4878.

Ritzwoller, M. H., N. M. Shapiro, M. P. Barmin, and A. L. Levshin (2002). Global surface wave diffraction tomography, *J. Geophys. Res.* **107,** 2335, doi: 10.1029/2002JB001777.

Rodi, W. L., P. Glover, T. M. C. Li, and S. S. Alexander (1975). A fast, accurate method for computing group-velocity partial derivatives for Rayleigh and Love modes, *Bull. Seismol. Soc. Am.* **65,** 1105–1114.

Shapiro, N. M., and M. H. Ritzwoller (2002). Monte-Carlo inversion for a global shear-velocity model of the crust and upper mantle, *Geophys. J. Int.* **151,** 88–105.

Shor, G. G., Jr., H. K. Kirk, and H. W. Menard (1971). Crustal structure of the Melanesian area, *J. Geophys. Res.* **76,** 2562–2586.

Simmons, N. A., S. C. Myers, G. Johannesson, and E. Matzel (2012). LLNL-G3Dv3: Global P wave tomography model for improved regional and teleseismic travel time prediction, *J. Geophys. Res.* **117,** no. B10302, doi: 10.1029/2012JB009525.

Takahashi, N., S. Kodaira, Y. Tatsumi, M. Yamashita, T. Sato, Y. Kaiho, S. Miura, T. No, K. Takizawa, and Y. Kaneda (2009). Structural variations of arc crusts and rifted margins in the southern Izu-Ogasawara arc-back arc system, *Geochem. Geophys. Geosyst.* **10,** no. Q09X08, doi: 10.1029/2008GC002146.

Takahashi, N., S. Kodaira, T. Tsuru, J.-O. Park, Y. Kaneda, K. Suyehiro, H. Kinoshita, S. Abe, M. Nishino, and R. Hino (2004). Seismic structure and sismogenesis off Sanriku region, northeastern Japan, *Geophys. J. Int.* **159,** 129–145.

Takeuchi, H., and M. Saito (1972). Seismic surface waves, in *Methods of Computational Physics*, B. A. Bolt (Editor), Vol. 11, Academic Press, New York, New York, 217–295.

Tarduno, J. A., W. V. Sliter, L. Kroenke, M. Leckie, H. Mayer, J. J. Mahoney, R. Musgrave, M. Storey, and E. L. Winterer (1991). Rapid formation of Ontong Java plateau by Aptian mantle plume volcanism, *Science* **254,** 399–403.

Trampert, J., and J. H. Woodhouse (2003). Global anisotropic phase velocity maps for fundamental mode surface waves between 40 and 150 s, *Geophys. J. Int.* **154,** 154–165.

Wessel, P., and W. H. F. Smith (1998). New, improved version of the Generic Mapping Tools released, *Eos Trans. AGU* **79,** 579.

Woodhouse, J. H., and F. A. Dahlen (1978). The effect of a general aspherical perturbation on the free oscillations of the Earth, *Geophys. J. Roy. Astron. Soc.* **53,** 335–354.

Woodhouse, J. H., and A. M. Dziewonski (1984). Mapping the upper mantle: Three-dimensional modeling of Earth structure by inversion of seismic waveforms, *J. Geophys. Res.* **89,** 5953–5986.

Xing, Z., and C. Beghein (2015). A Bayesian approach to assess the importance of crustal corrections in global anisotropic surface wave tomography, *Geophys. J. Int.* **203,** 1832–1846.

Zhu, H., E. Bozdağ, and J. Tromp (2015). Seismic structure of the European upper mantle based on adjoint tomography, *Geophys. J. Int.* **201,** 18–52.

Division of Geology and Geophysics
Kangwon National University
1 Gangwondaehak-gil, Chuncheon
Gangwon-do 24341, South Korea
sjchang@kangwon.ac.kr
(S.-J.C.)

Department of Earth Sciences
University College London
Gower Street
London WC1E 6BT, United Kingdom
(A.M.G.F.)

Manuscript received 8 May 2016;
Published Online 24 January 2017